The height of the current pulse was dependent on the recovery time from switching off the previous voltage step. For a recovery time of <100 ms no exoelectron emission could be detected; ~ 10 s was required for the pulse to be restored to its maximum height (Fig. 4). The height of the pulse increased with both applied voltage and temperature. Such pulses were detected at the lowest voltage of 3 kV. A ramped voltage (0 V to 10 kV at 300 V s^{-1}) gave no glow curve. We attribute this to the ease at which exoelectrons are emitted by electric fields and the existence of a steady-state emission current which would mask any glow curve.

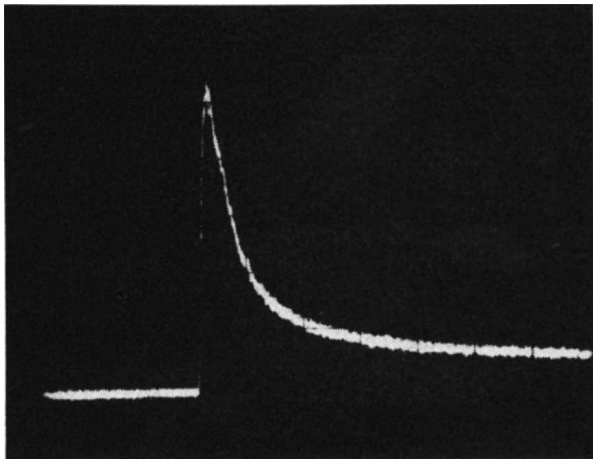

Fig. 3 Oscilloscope trace of the photomultiplier output of a burst of electrons from a single site, on stepping the emitter voltage from 0 V to 15 kV; 1 division on time axis = 0.5 s.

The connection between the exo and steady-state emission is still to be fully determined. Although steady-state emission may come from discrete energy levels in borosilicate glass[6] (there being no recognized conduction electrons), because of the slow, activated replenishment of exoelectrons, it is unlikely that the two types of emission occur from the same levels. Exoelectron emission has also been shown to depend strongly on surface conditions, and may disappear entirely in ultra-high vacuum[9]. Steady-state emission from glass is, however, maintained in ultra-high vacuum[7].

In conclusion, the pulse of electrons observed on applying a high voltage appears to be of exoelectrons; they are weakly held at the surface, and are only slowly replenished after emission. It should now be possible to investigate exoelectrons from other materials by the voltage step method. In particular, metals used as catalysts may be studied by this technique.

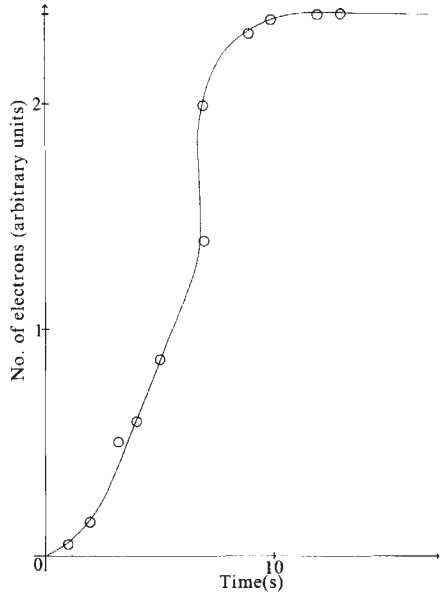

Fig. 4 Electron burst, measured as the height of the oscilloscope trace, as a function of the recovery time before a voltage step of 10 kV.

Received 8 February; accepted 12 March 1982.

1. Robertson, A. J. B. *Int. J. Electron* **51**, 607–619 (1981).
2. Balibar, F. *Recherche* **8**, 773–775 (1977).
3. Hoenig, S. A. & Utter, M. G. *J. Catal.* **47**, 210–213 (1977).
4. Shimida, H. & Nakajima, K. *Surface Sci.* **86**, 751–759 (1979).
5. Renfro, G. M. & Fishbeck, H. J. *Phys. Status Solidi* A**54**, 85–92 (1979).
6. Hibbert, D. B. & Robertson, A. J. B. *Proc. R. Soc.* A**349**, 63–79 (1976).
7. Hibbert, D. B. & Robertson, A. J. B. *Int. J. Electron* **48**, 301–303 (1980).
8. Hibbert, D. B. *27th int. Field Emission Symposium*, Tokyo, 138–139 (1980).
9. Kirihata, H. *Phys. Status Solidi* A**52**, K97–K99 (1979).

Helium isotopic systematics of oceanic islands and mantle heterogeneity

M. D. Kurz & W. J. Jenkins

Department of Chemistry, Woods Hole Oceanographic Institution, Woods Hole, Massachusetts 02543, USA

S. R. Hart

Center for Geoalchemy, Department of Earth and Planetary Science, Massachusetts Institute of Technology, Cambridge, Massachusetts 02139, USA

Isotopic variations in oceanic igneous rocks provide important constraints on models of oceanic mantle structure. Of particular interest is the global negative correlation between $^{87}Sr/^{86}Sr$ and $^{143}Nd/^{144}Nd$, which has been used to estimate 'bulk earth' values[1–3] for $^{87}Sr/^{86}Sr$, $^{87}Rb/^{88}Sr$ and $^{143}Nd/^{144}Nd$. Simple two-reservoir models have failed to explain all the isotopic variations, however, because of the complicated trends in Pb isotopes[4–6]. This has led to suggestions that recycled oceanic crust or sediments must be considered in these models[7–9]. We report here the results of helium isotopic analyses in basaltic phenocrysts from the islands of Gough and Tristan da Cunha. Because basalts from the islands lie near bulk earth on the Sr–Nd correlation diagram[3], the study was initiated to characterize the helium isotopic signature of this component. Whereas the ^3He in mantle gases is mostly primordial, the ^4He is primarily radiogenic, having been produced by decay of ^{238}U, ^{235}U and ^{232}Th. High $^3He/^4He$ ratios in igneous rocks therefore indicate primordial volatiles[10,11]. We believe that the present results are inconsistent with the notion that the mantle beneath Gough and Tristan da Cunha is primitive or undepleted relative to mid-ocean ridge basalt (MORB). Helium isotopic results on basaltic glasses and phenocrysts from the rift zone of Kilauea confirm the previously reported high values from this area[12–15]. We also report new analyses from Loihi Seamount (40 km south-east of Kilauea), which does seem to be derived from a more primitive source. When these data are combined with values for MORBs (from ref. 16) and plotted with respect to $^{87}Sr/^{86}Sr$, the observed trends offer insight into the different source regions for oceanic island basalts and the nature of mantle heterogeneity.

As sub-aerial basalts are largely degassed, they are of little use in the analysis of magmatic gas. This contrasts with MORB glasses, which are quenched rapidly enough on the ocean floor to trap substantial quantities of the magmatic gas[17,18]. Kaneoka *et al.*[12], however, have shown that the olivine phenocrysts from Kilauea basalts trap some of the magmatic gases that existed during crystal growth. The present results confirm the high $^3He/^4He$ ratios they reported for Kilauea phenocrysts, and we extend the approach to basalts from several other islands.

The samples were lightly crushed in a steel mortar, sieved, and the phenocrysts in the 20–40 mesh size range were separated by 'Frantz isodynamic' separation and hand-picking. Glassy samples were handpicked to exclude alteration, oxide

0028–0836/82/180043—05$01.00

crusts and non-vitreous chunks. Because the vesicles in submarine basalts can be a source of gas loss, chips >2 mm in size were selected[19]. After sonic cleaning, 1–2 g of the phenocrysts, or 400–500 mg of glass, were placed in a stainless-steel vessel designed specifically for *in vacuo* crushing[19]. The details of the gas mass spectrometry are similar to those reported earlier[19], except that the released helium was purified and expanded directly into the mass spectrometer, which resulted in a lower procedural blank ($1.0–2.0 \pm 0.3 \times 10^{-9}$ cm^3 STP ^{4}He with atmospheric ^{3}He/^{4}He). Due to the small sample size, variability in the blank is the primary contributor to the experimental uncertainty (see Table 1).

Strontium isotopic analyses of several of the samples were performed using techniques that have been described elsewhere[20]. The measured ^{87}Sr/^{86}Sr ratios for Loihi Seamount samples KK 20-4 and KK 23-3 were both 0.70358 ± 0.00002, and Staudigel *et al.*[21] reported a value of 0.70358 ± 0.00004 for sample KK18-8. Gough Island samples ALR 26G and ALR 41G had ^{87}Sr/^{86}Sr ratios of 0.70527 ± 0.00004 and 0.70521 ± 0.00005 respectively; the Prince Edward sample WJ21E had a ratio of 0.70305 ± 0.00004. These values are reported relative to an Eimer and Amend standard value of 0.70800; the errors are 2σ for in-run statistics.

The helium results are reported in Table 1 for phenocryst samples from Tristan da Cunha, Gough, Prince Edward, Jan Mayen and Kilauea. We also report the analyses of submarine basaltic glass from the Loihi Seamount and the east rift of Kilauea, and the rock type and sample source for each sample are listed; a more detailed description is given in ref. 22.

Examination of the phenocryst samples in thin section shows that the most likely residence site for the helium is in the ubiquitous melt inclusions. In most cases these inclusions have undergone some post-entrapment crystallization, which explains why most of the helium is released by crushing *in vacuo* (see Table 1). Crystallization excludes the gas from the melt, but helium is still trapped in the phenocryst. The absence of xenocrysts in these samples was verified by petrographical examination[22].

In testing whether phenocrysts can be used for gas analysis, the samples from Kilauea were chosen because they are well characterized, and because they allow comparison of the phenocryst helium with the magmatic helium. The good agreement between the phenocrysts from the Kilauea picrite (H66050) and the two submarine glasses from the same volcanic rift supports the use of phenocrysts to indicate magmatic ^{3}He/^{4}He ratios. Our results also confirm the relatively high ratios in Kilauea phenocrysts reported by Kaneoka *et al.*[12], and by several laboratories for the Kilauea fumaroles[13,14]. The Loihi samples have even higher ^{3}He/^{4}He ratios, up to 31.9 times atmospheric, but have ^{87}Sr/^{86}Sr ratios that are indistinguishable from the values for the Kilauea samples[23]. Note that Kaneoka and Takaoka[15] have reported even higher ^{3}He/^{4}He ratios (up to 37 times atmospheric) for phenocrysts from Haleakala (Maui).

In contrast, the Tristan da Cunha and Gough samples contain helium with ^{3}He/^{4}He ratios significantly lower than the MORB values. As it was impossible to separate the amphibole in TK 26 from the interstitial opaque oxides and other accessory minerals, and because there is some question about the origin of these gabbroic nodules[24], we also analysed a basalt from Tristan da Cunha that contained large phenocrysts (TK 46A). Special care was taken to avoid opaque oxides and possible host rock contaminants (U and Th rich phases). The similar ^{3}He/^{4}He ratio for two different phenocryst phases from the same sample (TK 46A and ALR 26G) and between different volcanic eruptions suggests that this is not a problem.

While Kilauea, Loihi Seamount, Tristan da Cunha and Gough all have ^{87}Sr/^{86}Sr ratios higher (more radiogenic) than MORB values, the Hawaiian samples have higher ^{3}He/^{4}He ratios and Tristan and Gough have lower ^{3}He/^{4}He ratios. As shown in the plot of ^{3}He/^{4}He against ^{87}Sr/^{86}Sr (Fig. 1), the results fall into two distinct trends. For reference, we also show MORB

Table 1 Helium isotopic analyses for phenocryst and glass samples

Sample	Phase analysed	Rock type and location	^{4}He cm^3 STP g^{-1}	σ	^{3}He/^{4}He (R/R_a)	σ	Sample source
Tristan da Cunha							
TK 26	Amphibole	Gabbro xenolith in pyroclastics, Buff Gulch	3.3×10^{-7}	0.1	5.2	0.1	†
*TK 26	Amphibole		1.0×10^{-7}	0.1	4.7	0.1	†
TK 46A	Olivine	Ankaramite, near Big Point	7.3×10^{-9}	0.8	6.3	0.7	†
*TK 46A	Olivine		1.0×10^{-9}	0.1	5.6	2.1	†
TK 46A	Clinopyroxene		3.5×10^{-8}	0.2	5.1	0.3	†
Gough Island							
ALR 41G	Clinopyroxene	Highly pyroxene phyric basalt, Mount Powett	1.3×10^{-9}	0.4	4.9	1.6	‡
*ALR 41G	Clinopyroxene		$<7.0 \times 10^{-10}$	—	—	—	‡
ALR 41G	Clinopyroxene		5.8×10^{-10}	0.9	5.5	0.7	‡
ALR 26G	Olivine	Ankaramite, Mount Powett	1.53×10^{-8}	0.06	6.2	0.2	‡
ALR 26G	Clinopyroxene		3.93×10^{-8}	0.09	6.2	0.3	‡
Jan Mayen							
JM 151A	Olivine	Ankaramite	—	—	6.3	0.5	§
	Clinopyroxene		9.7×10^{-9}	0.4	6.8	0.3	
Prince Edward							
WJ 21E	Olivine	Ankaramite, top of western escarpment	2.33×10^{-8}	0.05	7.4	0.2	‖
Kilauea							
H66050	Olivine	Picrite, crater wall	5.8×10^{-9}	0.3	14.0	1.4	¶
Puna 2	Glass	Tholeiite, East Rift	1.51×10^{-7}	0.03	14.7	0.5	#
Puna 8	Glass	Tholeiite, East Rift	1.88×10^{-7}	0.04	14.5	0.3	#
Loihi Seamount							
KK 23–3	Glass	Tholeiite	6.1×10^{-8}	0.04	23.1	0.8	††
KK 20–4	Glass	Alkali basalt	5.20×10^{-7}	0.14	24.1	0.7	††
KK 18–8	Glass	Tholeiite	2.71×10^{-7}	0.06	31.9	0.7	††

All samples were crushed *in vacuo* except those denoted*, which had the helium extracted by melting *in vacuo* after crushing. All ^{3}He/^{4}He ratios are reported relative to atmospheric (R/R_a) using an atmospheric value of 1.384×10^{-6}. Sample sources: †Dr S. Humphris; ‡Dr A. le Roex; §Dr S. Maaloe; ‖Dr W. J. Voerwoerd, see ref. 50; ¶Dr S. O. Agrell; #Dr J. Moore, see refs 51 and 23, sample numbers refer to Table 2 of ref. 51; ††Dr D. Clague, see ref. 52.

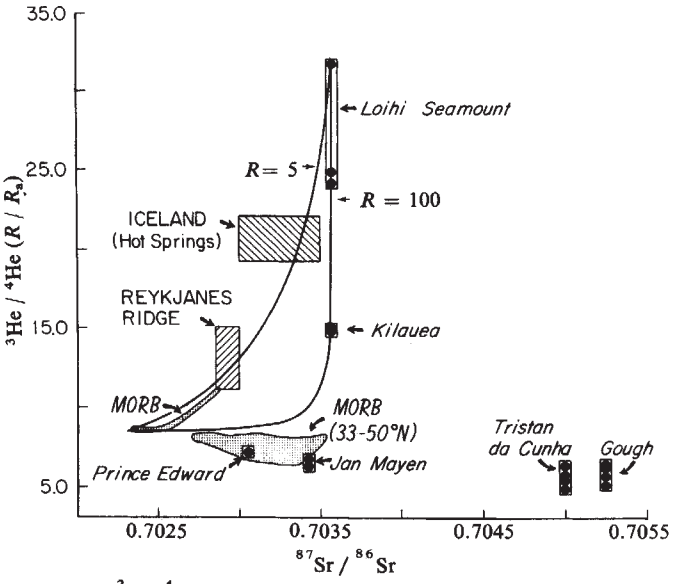

Fig. 1 $^3He/^4He$ (relative to atmosphere) plotted against $^{87}Sr/^{86}Sr$ for oceanic volcanic rocks. Data sources: Mid-Atlantic Ridge (MORB)[16]; Reykjanes Ridge[26,40]; Iceland[26,27,40,41]; Kilauea this study and ref. 23; Loihi Seamount, this study; Prince Edward, this study; Jan Mayen this study and ref. 42; Tristan da Cunha this study and ref. 3; Gough Island, this study. Note that the Gough, Prince Edward, MORB, Kilauea, and Loihi samples had helium and strontium isotopic analyses run on the same samples; in all other cases, the fields indicated represent ranges of values for similar samples from the references listed above. For the Icelandic hot springs, the highest reported $^3He/^4He$ ratios[26,27] were selected to minimize atmospheric effects. The highest terrestrial $^3He/^4He$ ratios (37 × atmospheric) reported by Kaneoka and Takaoka[15] are not plotted because they do not report $^{87}Sr/^{86}Sr$ ratios. The two mixing lines were calculated assuming component 1 has $^3He/^4He = 8.5 \times R_a$, $^{87}Sr/^{86}Sr = 0.70230$ and component 2 has $^3He/^4He = 32.0 \times R_a$, $^{87}Sr/^{86}Sr = 0.70358$. As shown by Langmuir *et al.*[28], curvature is determined by the ratio R, where in the present case:

$$R = \frac{^4He_1\ ^{86}Sr_2}{^4He_2\ ^{86}Sr_1}$$

with age of the Earth. This contrasts with continental crust, which is greatly enriched in U and Th and degassed of ^3He values for the North Atlantic, which are discussed in detail elsewhere[16], and literature values for Icelandic hot springs and the Reykjanes Ridge[25,26].

To explain these trends, we can immediately eliminate *in situ* (post-eruptive) decay of U and Th isotopes to produce the low $^3He/^4He$ trend, as all the samples are of essentially zero age and the phenocrysts analysed contain low U contents. This is also supported by the analyses of olivine and clinopyroxene from the same sample, which yielded similar results. We believe that the trends in Fig. 1 are most easily accounted for by three component mixing. One component, with $^3He/^4He$ of $\sim 1.17 \times 10^{-5}$ (8.5 × atmospheric) and $^{87}Sr/^{86}Sr$ of ~0.7025, would then be identified as the 'typical MORB' reservoir. A second component, characterized by high $^3He/^4He$ and higher $^{87}Sr/^{86}Sr$ ratios, would be consistent with a more primitive source derived from 'mantle plumes', as has been suggested for Hawaii and Iceland[15,27]. The third component is characterized by low $^3He/^4He$ and high $^{87}Sr/^{86}Sr$ ratios, as indicated by the results for Tristan and Gough.

The curve defined by the MORB–Loihi trend in Fig. 1 is consistent with mixing, as ratio–ratio plots do not always display straight lines for binary mixing[28]. Several mixing lines (calculated for different He and Sr concentrations in the end-members) are shown for reference in Fig. 1. The helium isotopic ratio of a possible primordial end-member (either 'planetary' or solar) is shown in Fig. 2. Because of the high He/(Th + U) ratio characteristic of the Sun and meteorites, there is little change in the $^3He/^4He$ ratio (due to addition of radiogenic ^4He) during formation, resulting in quite low present-day $^3He/^4He$ ratios (see Fig. 2). The primordial end-member would then lie between the Loihi seamount point and bulk earth as plotted in Fig. 2. Because it is not clear that there is a genetic relationship between the Earth and the meteorites, or whether any undifferentiated terrestrial mantle still exists, the true end-member must remain uncharacterized[16].

The low $^3He/^4He$ samples for Gough and Tristan da Cunha require mixing with a reservoir that has been enriched in Th and U relative to ^3He for time periods long enough to lower the $^3He/^4He$ ratio. The time required depends on the $^3He/(Th + U)$ ratio[16]. Our data cannot distinguish between seawater, subducted oceanic crust plus sediment, or old continental crust as a source for this component. As shown in Fig. 2, any of these would serve as an appropriate end-member if the mixing hypothesis is used to explain the variations. However, given the Sr–Nd correlation and the expected effect of seawater addition on these isotopes, seawater seems unlikely[29]. Seawater also contains small quantities of helium relative to basaltic melts, so addition of large quantities would be required to lower the $^3He/^4He$ ratio, and would result in extreme variations in $^{87}Sr/^{86}Sr$.

The suggestion[30] that an important source of isotopic variation in oceanic basalts is contamination from the oceanic crust through which the eruptive basalts must pass is plausible in that oceanic crust should separate ^3He from Th and U by degassing. However, this mechanism seems unlikely for several reasons. First, volcanics on Tristan da Cunha, Gough, Jan Mayen and Prince Edward are erupted through oceanic crust that is much younger (and thinner) that the crust beneath Hawaii, and yet the $^3He/^4He$ ratios are lowest. If contamination were significant, one would expect the oldest, most radiogenic crust to lower the ratio the most. Second, special conditions would be required to lower the magmatic $^3He/^4He$ ratio by this mechanism. The contaminating crust must have lost most of its initial He, and must have produced (and retained) substantial quantities of radiogenic ^4He. The generally low U and Th contents of unaltered oceanic crust require extreme enrichment in these

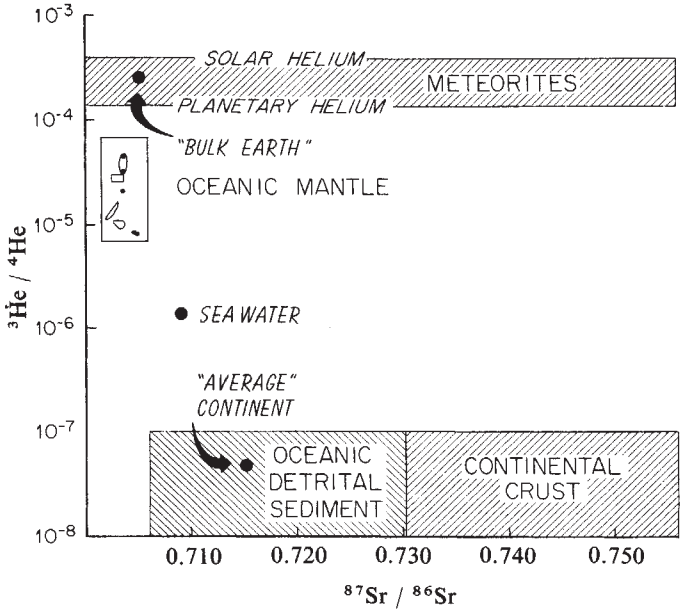

Fig. 2 Simplified plot of $^3He/^4He$ versus $^{87}Sr/^{86}Sr$ for terrestrial materials and meteorites. Data sources: chondrites[43,44]; bulk earth[3,44]; oceanic mantle (see Fig. 1); seawater[45,46]; continental shield[10,47]; oceanic detrital sediments[48]; and average crust[6,49]. Oceanic detrital sediments, and average crust are assumed to have the same range of $^3He/^4He$ ratios as continental gases[10]. We have also ignored meteoritic spallation helium, which can have $^3He/^4He$ ratios higher than 10^{-4}. The upper boundary for the oceanic mantle field is defined by helium analyses by Kaneoka and Takaoka[15].

elements to generate enough ^{4}He in reasonable time periods. This is particularly true for Tristan de Cunha and Gough, which are situated on oceanic crust that is 10–20 Myr old.

One mechanism that cannot be ruled out is the separation of He from U and Th by multiple melting events. For example, if the mantle beneath Tristan da Cunha and Gough were 'enriched' by the addition of a small amount of melt or fluid (equivalent to metasomatism[31]), it is conceivable that helium would be lost by degassing, while the U and Th would be retained. The ^{3}He/^{4}He ratio would then decrease, due to extremely low ^{3}He/U and ^{3}He/Th ratios; on melting, this enriched mantle would yield low ^{3}He/^{4}He ratios. Trace element analyses from Tristan da Cunha and Gough suggest that the lavas are enriched in Th and U relative to chondrites[32], making this feasible. However, the small degree of partial melting, which may generate oceanic island alkali basalts, makes it difficult to determine the source mantle characteristics from the trace element concentrations and ratios[33]. In addition, the physical process by which helium is lost from the mantle without melt removal is unclear.

The subduction of altered oceanic crust and sediments into the mantle has been suggested as an explanation for some of the Sr–Nd–Pb variations[7,8,34], and is quite consistent with our results for Tristan da Cunha and Gough. If the low ^{3}He/^{4}He, high ^{87}Sr/^{86}Sr mantle source region is produced by adding subducted crust into the mantle and then remelting, it is important to evaluate the effect on helium isotopes. The ^{3}He/^{4}He ratio that would result from remelting of this material is a function of the initial helium content of the crust, the amount of degassing it has undergone (both before and during subduction), the helium content of the mantle to which it is added, and the relative proportions of the two mantle types. These formidable uncertainties make a quantitative treatment impossible; however, there is clearly sufficient U and Th present to produce the observed variations, depending on the physical processes occuring. For example, in 200 Myr, 4×10^{-6} cm^{3}g^{-1} of radiogenic ^{4}He will accumulate in oceanic crust having an average U content of 100p.p.b. (parts per 10^9) and Th/U = 2 (ref. 35). If we take 1×10^{-5} cm^{3}g^{-1} as an upper limit of the initial helium content of oceanic crust, the ^{3}He/^{4}He ratio in this crust will decrease by at least 30% in 200 Myr. In addition, it is possible that hydrothermal alteration adds U to the crust, making 100 p.p.b. a lower limit[7,36,37]. The other extreme is an oceanic crust that degasses completely on formation, leaving only radiogenic ^{4}He to remix with the mantle on resubduction. Craig and co-workers[38] have interpreted low ^{3}He/^{4}He ratios in present-day back-arc volcanic systems to be a result of mixing between the helium in the downgoing slab and the helium in the underlying mantle, which suggests that degassing continues after crustal formation. In both cases, the ^{3}He/^{4}He will decrease to some extent, depending on the mixing ratio of the two components. Clearly, there is sufficient U and Th to lower the ^{3}He/^{4}He ratio significantly even before subduction. If the subducted crust remains in the mantle for long periods, as suggested by Hofmann and White[7], substantial quantities of radiogenic ^{4}He may accumulate.

All three mechanisms described above (crustal contamination, multiple melting, and remelting of subducted crust in the mantle) could conceivably produce the low ^{3}He/^{4}He trend defined by the Tristan da Cunha and Gough points. At present, we believe that the subducted crust hypothesis most easily accounts for the trend. In contrast to the other two processes, subduction is a commonly observed phenomenon. The mechanism for separation of He from U and Th is degassing of the oceanic crust, another presently observable phenomenon[14]. Further, the allowed time periods and U enrichments necessary to lower the ^{3}He/^{4}He ratio are geologically quite reasonable.

If all the high ^{3}He/^{4}He islands are produced by two component mixing with the same end-members, then various ^{4}He/^{86}Sr ratios are required, as this will determine the curvature of the mixing line. For example, if the Kilauea isotopic signature is derived by mixing the two end-members shown in Fig. 1, then the high ^{3}He/^{4}He end-member must have higher Sr contents or lower He contents (or both, see Fig. 1). Alternatively, another end-member may be involved. Note that Tatsumoto[35] observed different Pb isotopic compositions for each of the five sub-aerial Hawaiian volcanoes. He suggested that the linear trend, defined by the Hawaiian volcanoes, on the ^{207}Pb/^{204}Pb against ^{206}Pb/^{204}Pb plot was a mixing line. To test the mixing hypothesis, a more detailed study of the Loihi Seamount and the island of Hawaii is underway in our laboratories.

It would appear that ^{3}He/^{4}He measurements, coupled with the other isotopic measurements, are an important discriminant between primordial and 'recycled' mantle source regions. The reason for the large variations is that separation of He and Th + U occurs by degassing, which is not the case for the Rb–Sr, Nd–Sm, and U–Pb systems. Note that the samples lying close to bulk earth on the Nd–Sr correlation line, such as Tristan da Cunha and Gough, are not necessarily representative of undepleted mantle. It is possible to derive the trend by mixing between some crustal components[9,39] and the depleted MORB reservoir, resulting in a coincidental bulk earth value.

Therefore, on the basis of the helium isotopic information, three distinct mantle reservoirs are required: depleted (the MORB source), undepleted, and recycled. The islands displaying the highest ^{3}He/^{4}He ratios have tholeiitic affinities (Hawaii and Iceland), while the islands consisting of alkali basalts have characteristically lower ^{3}He/^{4}He ratios (Tristan da Cunha and Gough). More detailed sampling is required to confirm this trend.

We thank the following for providing samples: S. O. Agrell, D. Clague, S. Humphris, A. le Roex, S. Maaloe, J. Moore, R. K. O'Nions and W. Voerwoerd; also A. le Roex, G. Thompson, J.-G. Schilling and H. Dick for interesting discussions, and B. Haskell for editorial comments. M.K. thanks the Education Office of the WHOI/MIT Joint Program in Oceanography for their continuing support. This work was supported by NSF grant OCE–7909379 and USGS contract 14–08–001–G541. This is WHOI contribution no. 4955.

Received 24 August 1981; accepted 5 March 1982.

1. Richard, P., Shimizu, N. & Allègre, C. J. *Earth planet Sci. Lett.* **31,** 269 (1976).
2. DePaolo, D. J. & Wasserburg, G. J. *Geophys. Res Lett.* **3,** 249 (1976).
3. O'Nions, R. K., Hamilton, P. J. & Evensen, N. M. *Earth planet. Sci. Lett.* **34,** 13 (1977).
4. Sun, S. S. *Phil. Trans. R. Soc.* A**297,** 409–447 (1980).
5. Allègre, C. J., Brévart, O., Dupre, B. & Minster, J. F. *Phil. Trans. R. Soc.* A**297,** 447 (1980).
6. O'Nions, R. K., Evensen, N. M. & Hamilton, P. J. *J. geophys. Res.* **84,** 6091 (1979).
7. Hofmann, A. W. & White, W. M. *Yb. Carnegie Instn Wash.* 477–483 (1980).
8. Chase, C. G. *Earth planet. Sci. Lett.* **52,** 277–284 (1981).
9. Anderson, D. L. *Science* **213,** 82–89 (1981).
10. Tolstikhin, I. N. in *Terrestrial Rare Gases* (ed. Alexander, E. C.) (Center for Academic Publications, Japan, 1978).
11. Craig, H. & Lupton, J. in *The Sea* Vol. 7, 391–428 (Wiley, New York, 1981).
12. Kaneoka, I. & Takaoka, N. *Earth planet. Sci. Lett.* **39,** 382 (1978).
13. Craig, H. & Lupton, J. *Earth planet. Sci. Lett.* **31,** 369–385 (1976).
14. Jenkins, W. J., Edmond, J. M. & Corliss, J. B. *Nature* **272,** 156–158 (1978).
15. Kaneoka, I. & Takaoka, N. *Science* **288,** 1366–1368 (1980).
16. Kurz, M. D., Jenkins, W. J., Schilling, J.-G. & Hart, S. R. *Earth planet. Sci. Lett.* **58,** 1 (1982).
17. Funkhouser, J. G., Fisher, D. E. & Bonatti, E. *Earth planet. Sci. Lett.* **5,** 95–100 (1968).
18. Dymond, J. & Hogan, L. *Earth planet. Sci. Lett.* **20,** 131 (1973).
19. Kurz, M. D. & Jenkins, W. J. *Earth planet. Sci. Lett.* **53,** 41–54 (1981).
20. Hart, S. R. & Brooks, C. *Geochim. cosmochim. Acta* **38,** 1799–1806 (1974).
21. Staudigel, H. *et al. EOS* **62,** 1087 (1981).
22. Kurz, M. D. thesis, Woods Hole Oceanographic Inst./MIT Joint Program (1982).
23. Hart, S. R. *Earth planet. Sci. Lett.* **20,** 201–203 (1973).
24. Le Maitre, R. W. *Miner. Mag.* **37,** 185 (1969).
25. Polak, B. G., Komonmov, V. I., Tolstikhin, I. N., Mamyrin, B. A. & Khabarin, L. *Publ.* 119, *Int. Ass. Hydrol. Sci.*, 117 (1975).
26. Poreda, R., Craig, H. & Schilling, J.-G. *EOS* **61,** 1158 (1980).
27. Craig, H., Lupton, J. E., Welhan, J. & Poreda, R. *Geophys. Res. Lett.* **5,** 897 (1978).
28. Langmuir, C. H., Vocke, R. D., Hanson, G. N. & Hart, S. R. *Earth planet. Sci. Lett.* **37,** 380–392 (1978).
29. O'Nions, R. K., Carter, S. R., Cohen, R. S., Evenson, N. M. & Hamilton, P. J. *Nature* **273,** 435–438 (1978).
30. O'Hara, M. J. *Phil. Trans. R. Soc.* A**297,** 215–227 (1980).
31. Lloyd, F. E. & Bailey, D. K. *Phys. chem. Earth* **9,** 389–446 (1975).
32. Kable, E. J. thesis, Univ. Capetown (1974).
33. Gast, P. *Geochim. cosmochim. Acta* **32,** 1057 (1968).
34. Zindler, A. *Chapman Conf. on Oceanic Crust*, April (1981).
35. Tatsumoto, M. *Earth planet. Sci. Lett.* **38,** 63–87 (1978).
36. MacDougall, J. D. *Earth planet. Sci. Lett.* **35,** 65–70 (1977).
37. Mitchell, W. S. & Aumento, F. *Init. Rep. DSDP* Log **37,** 547–559 (1974).
38. Craig, H., Lupton, J. & Weiss, R. in *Terrestrial Rare Gases* (ed Alexander, E.) (Japan Scientific Society, Tokyo, 1978).
39. Carter, S. R., Evensen, H. M., Hamilton, P. J. & O'Nions, R. K. *Science* **202,** 743–747 (1978).
40. Hart, S. R., Schilling, J. G. & Powell, J. L. *Nature* **246,** 104 (1973).
41. Zindler, A., Hart, S., Frey, F. & Jakobbson, S. *Earth planet. Sci. Lett.* **45,** 249–262 (1980).

42. O'Nions, R. K. & Pankhurst, R. J. *J. Petrol.* **15,** 603 (1974).
43. Mittlefehldt, D. W. & Wetherill, G. W. *Geochim cosmochim. Acta* **43,** 201 (1979).
44. Heymann, D., in *Handbook of Elemental Abundances in Meteorites* (ed. Mason, B.) (Gordon & Breach, Edinburgh, 1971).
45. Clarke, W. B., Jenkins, W. J. & Top, Z. *Int. J. app. Rad. Isotopes* **27,** 515 (1976).
46. Faure, G. & Powell, J. L. *Strontium Isotope Geology* (Springer, Berlin, 1972).
47. McColloch, M. T. & Wasserburg, G. J. *Science* **200,** 1003–1011 (1978).
48. Dasch, E. J. *Geochim. cosmochim. Acta* **33,** 1521–1552 (1969).
49. Hart, S. R. & Allegre, C. J. in *Physics of Magnetic Processes* (ed. Hargreaves, R.) 121–151 (Princeton University Press, 1980).
50. Voerwoerd, W. J. in *Marion and Prince Edward Islands* (eds Van Zinderen, E. M. *et al.*) (Balkema, Capetown, 1971).
51. Moore, J. G. *Am. J. Sci.* **263,** 40–52 (1965).
52. Moore, J., Claque, D. & Normark, W. *Geology* **10,** 88–92 (1982).

Scaling rules in rock fracture and possible implications for earthquake prediction

C. J. Allegre, J. L. Le Mouel & A. Provost

Institut de Physique du Globe, Université Paris 6, 2 place Jussieu, Paris 75005, France

A major preoccupation in physical sciences has been to interpret macroscopic events from microscopic phenomena. In some cases the change of scale is efficient and fairly easy to perform, but in others it turns out to be difficult and uninteresting. Success or failure is due more to the nature of the events than to the efficiency of the theoretical methods used. Some macroscopic phenomena have their origin in a microscopic organization which can be transferred to larger scales whereas others attain their structure on the macroscopic scale itself. Thus before applying scaling laws techniques[1–4] one must ensure that embedded scales are suggested by physical observations. That this seems to be the case for the fracture of rocks is supported by geological, seismological and rock mechanics observations. We have therefore built a very simple model based on scaling laws which yields a criterion for fragility at different scales and views rupture as a critical point. We use this model here to outline a general approach to earthquake prediction.

Fracturing occurs in rocks at all scales, from the microscale (microcracks) to the continental scale (megafaults), and the geologist can equally well observe embrittlement and rupture phenomena under the microscope as on satellite photographs (Fig. 1). But are the various scales of fracture related to one another? The following observations suggest they are: (1) field geologists know that the great faults of the crust—such as the San Andreas fault—actually consist of anastomosed faults, sometimes arranged *en échelon*, thus weakening a whole domain of the crust, down to variable depths[5]. (2) Seismologists who study source phenomena often have to introduce in their models complex rather than single faults, each one contributing to the observed radiation pattern[6,7]. (3) Rock mechanicists, when studying fracture in the laboratory, observe that it is preceded by the concentration of a swarm of microfissures which are themselves the result of an accumulation of microcracks[8–11]. From this set of observations one can suggest that fracture at the macroscopic scale is a consequence of accumulations of ruptures at lesser scales.

This hypothesis has been actually adopted by Brace and his students[8,9,11,12]. They have submitted rock samples to progressive triaxial loading ($\sigma_1, \sigma_2, \sigma_3$) and studied the increase of microcrack density with increasing load. This increase seems to be the result of two distinct processes: (1) the nucleation of new cracks, that is, the birth of new rupture points in the material; and (2) the growth of pre-existing cracks. In fact, as noted by Brace *et al.*[8] and Tapponnier and Brace[11], the nucleation seems to occur most often from a pre-existing crack. The distinction between the two processes is thus subtle and the increase in crack density can be considered to be ruled by a single phenomenon with a given activation energy.

The law governing the increase of microcrack density with deviatoric stress ($\sigma_1 - \sigma_3$) depends strongly on the confining pressure. But what seems to occur generally is that the macroscopic fracture is not preceded by an accelerated growth of microcrack density as measured over the whole sample. When the sample is examined at different scales one observes that cracks collect in some regions, but that these microscopic regions are roughly homogeneously distributed in the medium, even when the rupture threshold has been reached. On the other hand, the larger the scale the stronger is the spatial heterogeneity. The heterogeneity reaches, of course, a limit which determines the fracture itself whose orientation follows the laws established by Anderson[13].

We will now try to explain those observations with a simple renormalization group (RG) model and examine possible implications of the model for earthquake prediction.

For each elementary domain of rock (say 100 μm), we define two states: when the local microcrack density in the domain is greater than some critical value, it is considered as fragile (f); otherwise it is considered as sound (s).

As shown elsewhere (for example, see ref. 11), the mean microcrack density d depends linearly on $(\sigma_1 - \sigma_3)$ (for a given σ_2), but the local density varies considerably within the sample. The probability for an elementary domain to be fragile, p, is directly proportional to d and thus linearly related to $(\sigma_1 - \sigma_3)$ (for a given σ_2):

$$d = d_0 + b(\sigma_1 - \sigma_3)$$
$$p = ad = ad_0 + ab(\sigma_1 - \sigma_3) \quad (1)$$

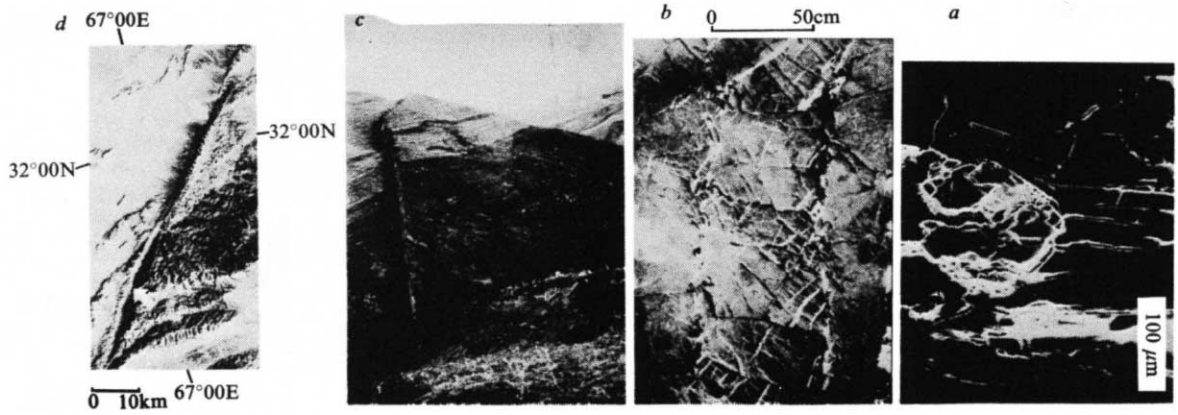

Fig. 1 Examples of fracture at different scales. *a*, Microcracks in quartz grains are induced by intense cracking in magnetite and plastic flow in biotite. (Westerly granite, fracture stress, 35 bar of confining pressure, room temperature.) *b*, Tension gashes, stylolites and micro shear faults in horizontal Mesozoic limestones (near Les Matelles, in Languedoc, France). The microstructures combine to form a fault zone at a larger scale. *c*, Master fault of the El Asnam, Algeria, earthquake (magnitude = 7.3, 10 October 1980). In the hills north of El Attaf, the break, several kilometres long, has up to 4 m of vertical throw. *d*, Landsat image of the Chaman strike-slip fault south-west of the Katawaz basin near the border between Afghanistan and Pakistan. The fault system, ~1,200 km long, may have accommodated as much as 500 km of left lateral displacement of India past Afghanistan in the past 40 Myr.

0028-0836/82/180047—03$01.00